Floating Tristate Double Boost Converter and a Modification

FELIX A. HIMMELSTOSS

Faculty of Electronic Engineering and Entrepreneurship,
University of Applied Sciences Technikum Wien,
Hoechstaedtplatz 6, 1200 Vienna,
AUSTRIA

Abstract: - Two concepts are combined in this paper. First, the tristate concept, where the electronic switch of a DC/DC converter is replaced by a combination of two electronic switches and an additional diode. This leads to two interesting features: first the voltage-transformation ratio can be linearized and second the system can be transferred into a phase minimum system, which makes the control easier. The second two tristate Boost converters are combined to a floating double Boost converter. The basic function of the converter is explained. The large and the linearized small signal models are derived, transfer functions calculated, and Bode plots drawn. The dynamic behavior is studied with transfer functions and by circuit simulations done with LTSpice. The inrush is studied and a modification of the converter is shown to avoid dangerous overcurrents.

Key-Words: - Boost converter, floating converter, tristate converter, modified converter, modeling, large signal model, linearization, small signal model, transfer function.

1 Introduction

The starting point of these investigations is the floating double Boost converter as shown in Figure 1.
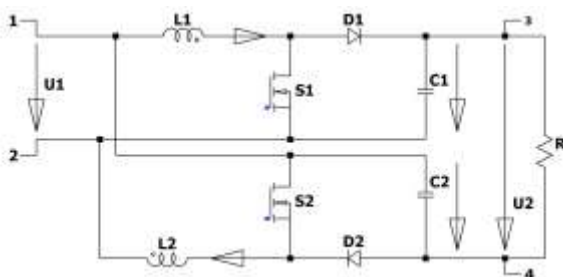
Fig. 1: Floating double Boost converter

The converter consists of two Boost converters, each realized by a coil, a switch, a diode, and a capacitor. The two converters are connected in parallel at the input and work in series at the output. At terminals 1 and 2 the input voltage source is connected. The load is applied to the terminals 3 and 4. One can immediately see that the output voltage is given by the voltage across the two output capacitors of the two Boost converters minus the input voltage:

$$U_2 = U_{C1} + U_{C2} - U_1 . \qquad (1)$$

The voltage-time balance across the inductors (we use a symmetrical design and control both active switches with the same duty cycle) in the steady state is given by:

$$U_1 \cdot d = |U_1 - U_C|(1-d) \qquad (2)$$

which leads to the voltage across the capacitors:

$$U_{C1} = U_{C2} = \frac{U_1}{1-d} . \qquad (3)$$

With (1) and (3) the voltage transformation ratio is obtained according to:

$$M = \frac{U_2}{U_1} = \frac{1+d}{1-d} . \qquad (4)$$

The circuit diagram of the floating double Boost converter can be found in [1], [2], [3], [4], [5]. In [1], the converter is used for a photovoltaic system and combined with a robust control. The application shown in [2], is a combined fuel-cell and supercapacitor system. In [3], an observer system is applied to the converter. [4], shows again fuel cells as a supply and in [5], the converter supplies a DC micro-grid. In [6], [7] and [8], the converter is combined with the interleaved concept for each Boost part. [9], uses additional resonant circuits. In [10], the diodes are replaced by electronic switches. So a bidirectional operation is possible.

2 Floating Tristate Double Boost Converter

The floating double converter concept (one can use other converter stages instead of the Boost) is now combined with the tristate concept. Here the active switch is replaced by a series connection of two active switches S1, S2, and a diode D1 which is joined to the connection point of the two electronic switches. The other terminal of the diode is connected to the coil. Figure 2 shows this concept applied to the floating double-boost converter. The tristate concept goes back to [11], and is deepened in [12] and [13]. The concept can be extended to a bidirectional one, [14], [15]. So energy flow in both directions is possible and the onward losses can be reduced. An improvement to reduce the switching losses is presented in [16]. The tristate concept is mainly applied to the Boost converter. In [17], the tristate concept is not only applied to the Buck and the Boost converters, but also to the Buck-Boost, the Cuk, the Sepic, the Zeta, the D-square, the (2d-1)/(1-d), and to the improved super-lift Boost converters.
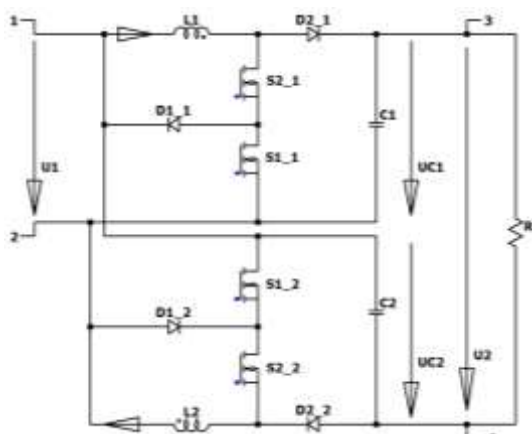
Fig. 2: Floating tristate double Boost converter

In the continuous inductor current mode, the tristate converter has three modes. In mode M1 both active switches are turned on and the input voltage is across the inductor, in mode M2 S1 is turned off and the inductor is short-circuited by S2 and D1. The current through the coil stays now nearly constant. In mode M3 S2 is off and only D2 is on. Now a negative voltage is across the coil and the current through it decreases.

The voltage-time balance of a Boost part can be written according to:

$$U_1 d_1 = |U_1 - U_C|(1 - d_2) \qquad (5)$$

which leads to the voltage transformation ratio:

$$\frac{U_C}{U_1} = \frac{1 + d_1 - d_2}{1 - d_2} \ . \qquad (6)$$

The voltage transformation ratio of the whole converter is therefore:

$$\frac{U_2}{U_1} = 2\frac{1 + d_1 - d_2}{1 - d_2} - 1 = \frac{1 + 2d_1 - d_2}{1 - d_2} \qquad (7)$$

with the limitation

$$d_2 \geq d_1 . \qquad (8)$$

The voltage transformation ratio with constant duty cycle d2 and variable duty cycle d1 is shown in Figure 3. The transformation ratio is linearized and higher compared to the normal floating double boost converter (FDBC) without the tristate concept.
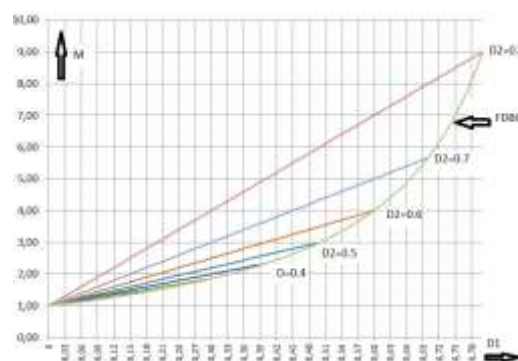
Fig. 3: Floating tristate double Boost converter, voltage transformation ratio: duty cycle of S2 as a parameter and duty cycle of S1 as independent variable

The voltage transformation ratio with constant duty cycle d1 and variable duty cycle d2 is shown in Figure 4. The transformation is lower compared to the normal floating double boost converter (FDBC) without the tristate concept, and the curvature is smaller.
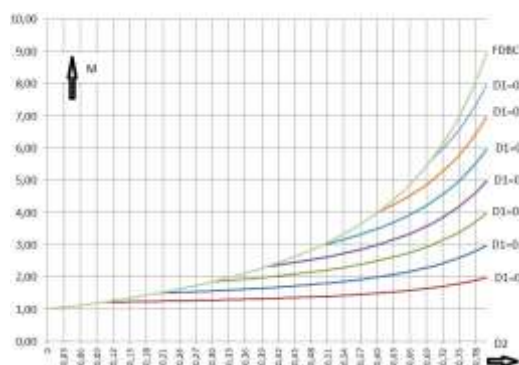
Fig. 4: Floating tristate double Boost converter, voltage transformation ratio: duty cycle of S1 as a parameter and duty cycle of S2 as independent variable

Figure 5 shows the converter in the steady state. The current through the coils and the load current are shown in the upper graph. In the lower graph the output, the input voltages, and the control signals of the switches are shown. The two converter stages are controlled in an interleaved way, the signals of the second stage are shifted by 180 compared to those of the other stage.

The tristate converter suffers again from the inrush current when applied to a stiff input voltage. The inrush is equal to the one of the normal floating double Boost converter.
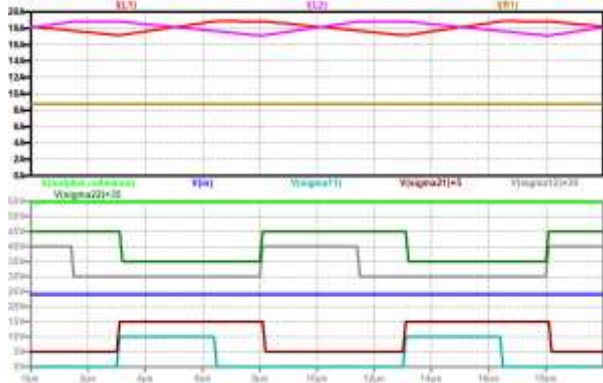
Fig. 5: Tristate floating Boost converter, up to down: Current through L1 (red), current through L2 (violet), load current (brown); output voltage (green), the control signal of S2_2 (dark green, shifted), the control signal of S1_2 (grey, shifted); control signal of S2_1 (black), the control signal of S1_1 (turquoise)

3 Model of the Converter

3.1 State-space Models

The two stages are built similarly and both converter stages are controlled by the same duty cycles. The converter can now be described by a second-order system! So it is not necessary to distinguish between the inductors and the capacitors, one can write only L for the coils and C for the capacitors. The load current can be written according to:

$$i_{LOAD} = \frac{2u_C - u_1}{R} \ . \qquad (9)$$

During mode M1 both active switches of the stages are turned on and the state equations for the change of the current through the inductors and the change of the voltage across the capacitors are:

$$\frac{di_L}{dt} = \frac{u_1}{L}, \qquad \frac{du_C}{dt} = \frac{(-2u_C + u_1)/R}{C} \ . \quad (10)$$

For the mode M2 (S1 is turned off and D1 turns on) one gets:

$$\frac{di_L}{dt} = 0 \ , \qquad \frac{du_C}{dt} = \frac{(-2u_C + u_1)/R}{C} \ . \quad (11)$$

When the second electronic switch S2 is turned off, D2 turns on and D1 turns off, and the describing state equations are:

$$\frac{di_L}{dt} = \frac{u_1 - u_C}{L} \ , \qquad \frac{du_C}{dt} = \frac{i_L + (-2u_C + u_1)/R}{C} \ .$$
(12)

To get the weighted model of the converter one has to weigh the equations of the three modes by d1, d2-d1, and 1-d2, respectively, and add them. This leads to the large signal model:

$$\frac{d}{dt}\begin{pmatrix} i_L \\ u_C \end{pmatrix} = \begin{bmatrix} 0 & \dfrac{d_2 - 1}{L} \\ \dfrac{1 - d_2}{C} & -\dfrac{2}{RC} \end{bmatrix}\begin{pmatrix} i_L \\ u_C \end{pmatrix} + \begin{bmatrix} \dfrac{1 + d_1 - d_2}{L} \\ \dfrac{1}{RC} \end{bmatrix}(u_1) .(13)$$

Linearizing leads to the small signal model:

$$\frac{d}{dt}\begin{pmatrix} \hat{i}_L \\ \hat{u}_C \end{pmatrix} = \begin{bmatrix} 0 & \dfrac{D_2 - 1}{L} \\ \dfrac{1 - D_2}{C} & -\dfrac{2}{RC} \end{bmatrix}\begin{pmatrix} \hat{i}_L \\ \hat{u}_C \end{pmatrix} +$$

$$+ \begin{bmatrix} \dfrac{1 + D_{10} - D_{20}}{L} & \dfrac{U_{10}}{L} & \dfrac{U_{C0} - U_{10}}{L} \\ \dfrac{1}{RC} & 0 & -\dfrac{I_{L0}}{C} \end{bmatrix}\begin{pmatrix} \hat{u}_1 \\ \hat{d}_1 \\ \hat{d}_2 \end{pmatrix} . \quad (14)$$

The connections at the operating point are:
$$(D_{20} - 1)U_{C0} + (1 + D_{10} - D_{20})U_{10} = 0 \qquad (15)$$

resulting in:

$$U_{C0} = \frac{1 + D_{10} - D_{20}}{1 - D_{20}}U_{10} \qquad (16)$$

$$(1 - D_{20})I_{L0} - \frac{2}{R}U_{C0} + \frac{1}{R}U_{10} = 0 \qquad (17)$$

leading to:

$$I_{L0} = \frac{2U_{C0} - U_{10}}{R(1 - D_{20})} = \frac{I_{LOAD}}{1 - D_{20}} \ . \qquad (18)$$

Using abbreviations for the elements of the state and the input matrixes leads to the Laplace transformed system for the coil current and the voltage across the capacitors in the s-domain according to:

$$\begin{bmatrix} s & -A_{12} \\ -A_{21} & s - A_{22} \end{bmatrix}\begin{pmatrix} I_L(s) \\ U_C(s) \end{pmatrix} + \begin{bmatrix} B_{11} & B_{12} & B_{13} \\ B_{21} & 0 & B_{23} \end{bmatrix}\begin{pmatrix} U_1(s) \\ D_1(s) \\ D_2(s) \end{pmatrix}$$

(19)

The output voltage is given (in the time-domain) by:

$$u_2 = \begin{bmatrix} 0 & 2 \end{bmatrix} \begin{pmatrix} i_L \\ u_C \end{pmatrix} + \begin{bmatrix} -1 \end{bmatrix}(u_1). \qquad (20)$$

All six possible describing transfer functions have the same denominator:

$$Den = s^2 - A_{22} \cdot s - A_{12}A_{21} = (s+\delta)^2 + \omega^2 \qquad (21)$$

The damping factor and the angular resonant frequency can now be written by:

$$\delta = \frac{A_{22}}{2} \text{ and } \omega = \sqrt{A_{12}A_{21} - \delta^2} \qquad (22)$$

and with the parameters of the converter to:

$$\delta = \frac{1}{RC} \text{ and } \omega = \sqrt{\frac{(1-D_{20})}{LC} - \frac{1}{R^2C^2}}. \qquad (23)$$

The smaller R and C the better the system is damped and the ringing is reduced.

The parameters of the converter are L=47 µH, C=330 µF, R=6.25 Ω, and the working point is described by U10=24 V, UC0=39.8 V, IL0=17.5 A, D10=0.33, D20=0.5. All Bode plots and step responses are calculated with these values. The damping factor is $\delta = \frac{1}{RC} = 484$ and the angular frequency is $\omega = 3986\,\text{s}^{-1}$ and the frequency 634 Hz.

3.2 Transfer Functions

Now the numerators of the transfer functions have to be calculated.

3.2.1 UC(s) in Dependence on D1(s)

The numerator can be found by:

$$Num\_UCD1 = \begin{vmatrix} s & B_{12} \\ -A_{21} & 0 \end{vmatrix} = A_{21}B_{12}. \qquad (24)$$

The transfer function is a simple second-order phase-minimum system and the phase tends asymptotically to -180°. The damped ringing is caused by the poles. Figure 6 shows the Bode plot and Figure 7 the step response. The resonance is in good coincidence with the calculation.
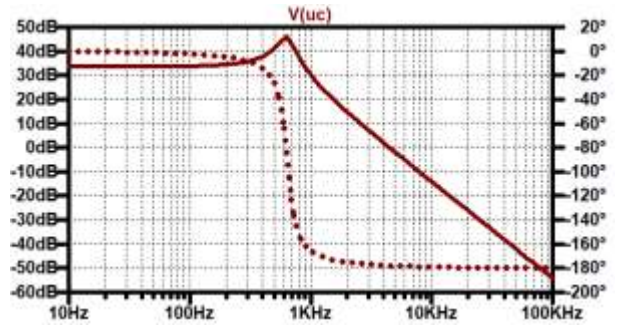
Fig. 6: Transfer function between capacitor voltage and duty cycle of switch S1: Bode plot (solid line: gain response, dotted line: phase response)
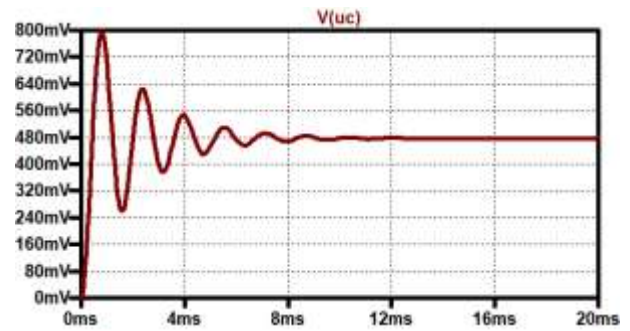
Fig. 7: Transfer function between capacitor voltage and duty cycle of switch S1: step response (1 %)

3.2.2 UC(s) in dependence on D2(s)

The numerator is now a first-order function

$$Num\_UCD2 = \begin{vmatrix} s & B_{13} \\ -A_{21} & B_{23} \end{vmatrix} = s \cdot B_{23} + A_{21}B_{13}. \qquad (25)$$

B_{23} is negative. The zero is therefore on the right side of the complex plane

$$s_Z = -\frac{A_{21}B_{13}}{B_{23}} = \frac{(U_{C0}-U_{10})(1-D_{20})}{I_{L0}L} \qquad (26)$$

and the converter is, like other step-up converters, described by a non-phase minimum system.

The zero on the right side shifts the phase of the system to another -90 at high frequencies to -270° and leads to a slower controlled system. The higher the value of the coil, the nearer the zero at the imaginary axis, and the greater the influence of the zero. Figure 8 shows the Bode plot and Figure 9 the step response for a change of the duty cycle of 1 %. The response starts first in the wrong direction, the voltage reduces first and increases a little bit later. This is typical for systems with zeros on the right side.
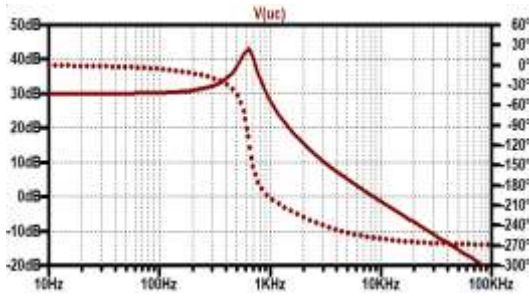
Fig. 8: Transfer function between capacitor voltage and duty cycle of switch S2: Bode plot (solid line: gain response, dotted line: phase response)
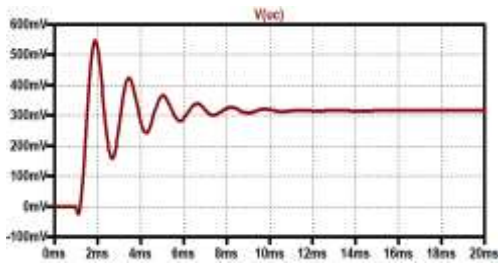
Fig. 9: Transfer function between capacitor voltage and duty cycle of switch S2: step response (1 %)

For a simpler control (the plant is a phase minimum system) it is useful to control the converter with d1 and d2 fixed. The duty cycle of S1 must be lower than or equal to the duty cycle of S2.

3.2.3 UC(s) in Dependence on U1(s)

The numerator of the transfer function between the voltage across the capacitor and the input voltage:

$$Num\_UCU1 = \begin{vmatrix} s & B_{11} \\ -A_{21} & B_{21} \end{vmatrix} = s \cdot B_{21} + A_{21}B_{11} \qquad (27)$$

leads to a zero on the left side of the complex plane at :

$$s_Z = -\frac{A_{21}B_{11}}{B_{21}} = -\frac{(U_{C0} - U_{10})(1 - D_{20})R}{L} \qquad (28)$$

and to a phase minimum system. The phase tends now to only -90° at higher frequencies. Figure 10 shows the Bode plot and Figure 11 the step response.

This transfer function is especially necessary when a disturbance feedforward is applied.
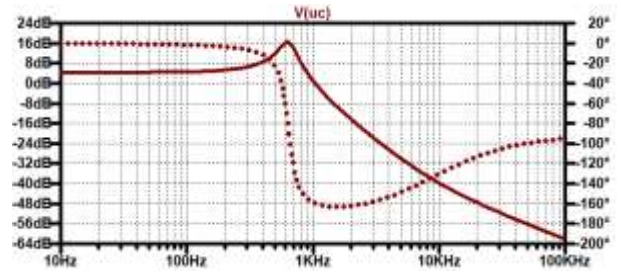
Fig. 10: Transfer function between capacitor voltage and the input voltage: Bode plot (solid line: gain response, dotted line: phase response)
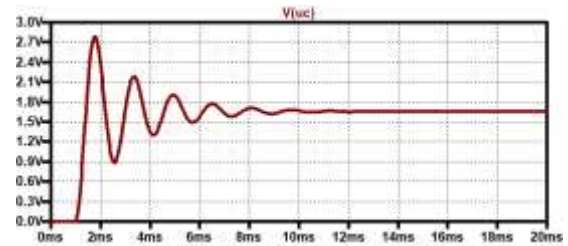
Fig. 11: Transfer function between capacitor voltage and the input voltage: step response (1 V)

Sometimes the control of the current through the coil is of importance e.g. by using the converter for supplying light emitting diodes, or when using a two-loop control.

3.2.4 IL(s) in Dependence on D1(s)

The numerator of the current through the inductor and the duty cycle of switch S1 can be calculated according to:

$$Num\_ILD1 = \begin{vmatrix} B_{12} & -A_{12} \\ 0 & s - A_{22} \end{vmatrix} = B_{12} \cdot s + A_{22}B_{12}. \qquad (29)$$

The zero is at:

$$s_Z = -A_{22} = \frac{2}{CR} \quad (967 \text{ s}^{-1}, 154 \text{ Hz}) \qquad (30)$$

and is at the left side of the complex plane and the phase tends now to only -90°. The control is therefore easy. Figure 12 shows the Bode plot and Figure 13 the step response.
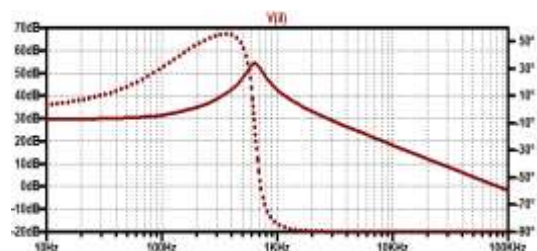
Fig. 12: Transfer function between the current through the coil and the duty cycle of switch S1: Bode plot (solid line: gain response, dotted line: phase response)
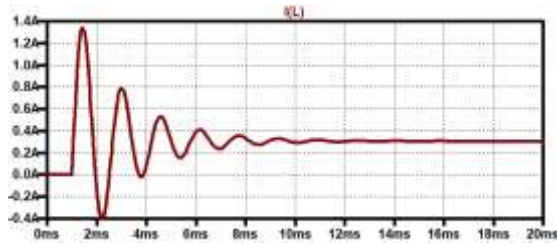
Fig. 13: Transfer function between the current through the coil and the duty cycle of switch S1: step response (1 %)

3.2.5 IL(s) in Dependence on D2(s)

The numerator of the transfer function between the current through the coil and the duty cycle of switch S2 can be found in

$$Num\_ILD2 = \begin{vmatrix} B_{13} & -A_{12} \\ B_{23} & s-A_{22} \end{vmatrix} = B_{13} \cdot s - A_{22}B_{13} + A_{12}B_{23}$$

(31)

The zero lies at

$$s_Z = \frac{A_{22}B_{13} - A_{12}B_{23}}{B_{13}} = -\frac{2}{RC} - \frac{(1-D_2)I_{L0}}{(U_{C0} - U_{10})C} \quad (32)$$

and again the transfer function describes a phase minimum system. Figure 14 shows the Bode plot and Figure 15 shows the step response.
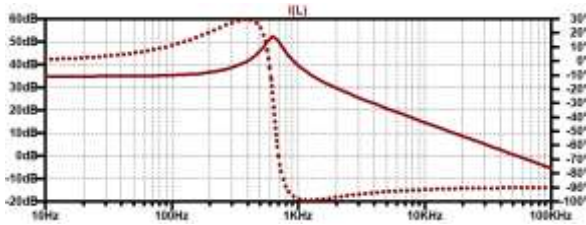
Fig. 14: Transfer function between the current through the coil and the duty cycle of switch S2: Bode plot (solid line: gain response, dotted line: phase response)
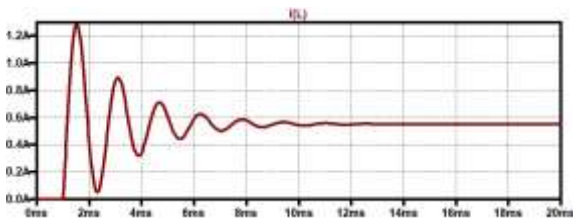
Fig. 15: Transfer function between the current through the coil and the duty cycle of switch S2: step response (1 %)

3.2.6 IL(s) in Dependence on U1(s)

The numerator of the transfer function between the current through the coils and the input voltage is obtained by:

$$Num\_ILU1 = \begin{vmatrix} B_{11} & -A_{12} \\ B_{21} & s-A_{22} \end{vmatrix} = B_{11} \cdot s - A_{22}B_{11} + A_{12}B_{21}$$

(33)

The zero is again on the left side at

$$s_Z = \frac{A_{22}B_{11} - A_{12}B_{21}}{B_{11}} = -\frac{2}{RC} - \frac{2(1-D_{20})}{(1+D_{10}-D_{20})CR} \quad . \quad (34)$$

Figure 16 shows the Bode plot and Figure 17 the step response.
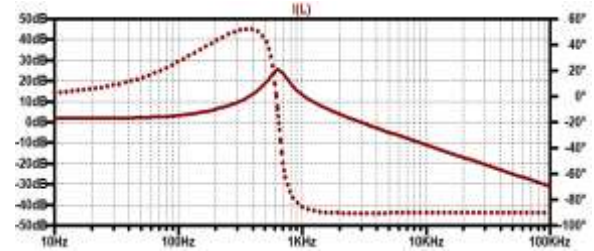
Fig. 16: Transfer function between the current through the coil and the input voltage: Bode plot (solid line: gain response, dotted line: phase response)
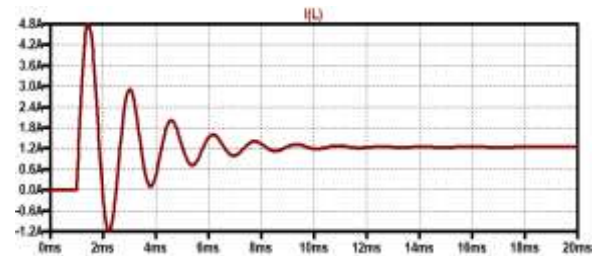
Fig. 17: Transfer function between the current through the coil and the input voltage: step response (1 V)

The control of the current is easy for all three input variables and can be done by a PI controller. In a two-loop control, only a P-controller for the inner current loop is necessary. More results are shown in section 6.

4 Inrush

A very important aspect of a converter is its inrush current when the input voltage is applied. This is especially important when the input source is stable and can deliver a large current.

Figure 18 shows an inrush when the converter is applied at 24 V (the used converter parameters are L1=L2=47 µH, C1=C2=330 µF). The input voltage goes up within 10 µs. The currents through the coils rise nearly sinusoidal (damped by the load resistor), and when the current reaches zero the diodes turn off. The voltage across the capacitors rises to nearly

double the input voltage, then the capacitors are discharged by the load (with an exponential function). When the voltage across a capacitor is lower than the input voltage by a forward voltage of the diode, the diode turns on and recharges the capacitor with a damped sinusoidal waveform. The current through the load is supplied by both converter stages. From the load current one can imply that the output voltage is negative at the beginning.
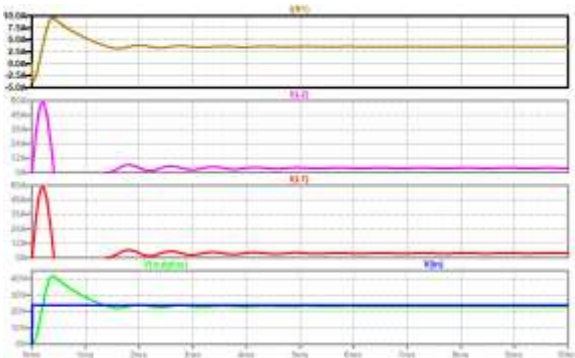
Fig. 18: Tristate floating double Boost converter: inrush with load resistor 6.25 Ω, up to down: load current (brown); current through L2 (violet); current through L1 (red); voltage across C1 (green), input voltage (blue)

Figure 19 shows the inrush when no load is connected to the converter. The converter parameters are the same as for Figure 18. The current through the inductors are sinusoidal half-waves. The voltage across the load becomes negative until the capacitors are charged so that they can compensate for the input voltage. The voltage across the capacitors reaches nearly two times the input voltage. (Without losses across the diode and the series resistors of the coil and the capacitor, it would reach double the input voltage exactly).
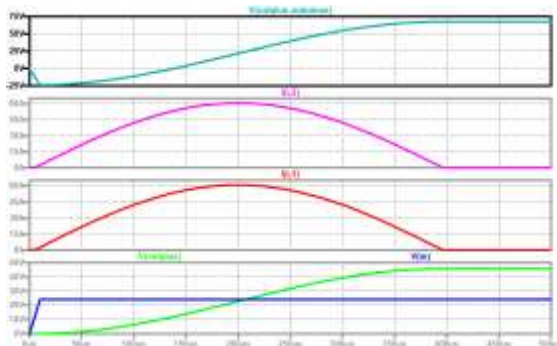
Fig. 19: Tristate floating double Boost converter: inrush with no load, up to down: output voltage (turquoise); current through L2 (violet); current through L1 (red); voltage across C1 (green), input voltage (blue)

This converter has a large inrush current when connected to a stiff input voltage, as are batteries and DC microgrids. The inrush current is two times the resonant current of the resonant circuit formed by the coil and the capacitor of a converter leg leading to

$$\hat{I}_{IN} = 2\sqrt{\frac{C}{L}}U_1 \; . \tag{35}$$

One should also keep in mind that the inductor will saturate and decrease and so the current will get much higher!

With an additional input transistor SIN which starts with a duty cycle from zero and increases to one by a ramp function, the current into the converter can be reduced and controlled. This additional transistor SIN can also be used as a fuse to turn off the converter very fast in the case of a short-circuit, open circuit, overcurrent, or overheat. Between the drain of the transistor SIN and the anode of the additional diode DIN, an input capacitor CIN has to be connected (Figure 20). Figure 21 shows the turn-on with no load and Figure 22 with load. The current through L1 is depicted, the current through the other coil looks equal, and the input current is therefore double as large. The output voltage, the voltages across the capacitors, and the input voltage are also shown in these figures. No dangerous current occurs, but the output voltage is negative again at the beginning.
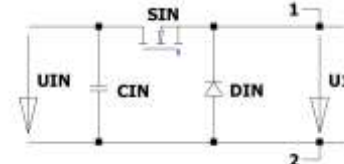
Fig. 20: Pre-stage to avoid the inrush and to serve as an electronic fuse
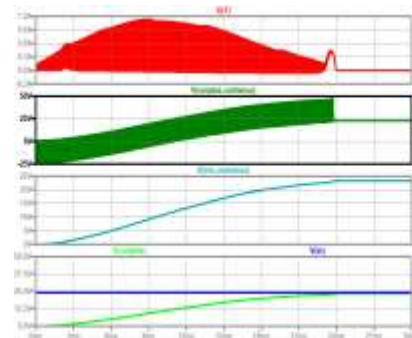
Fig. 21: Floating double Boost with additional inrush current reduction (no load), up to down: current through the first coil (red); output voltage (dark green); the voltage across the second capacitor (turquoise); input voltage (blue), voltage across the first capacitor (green)
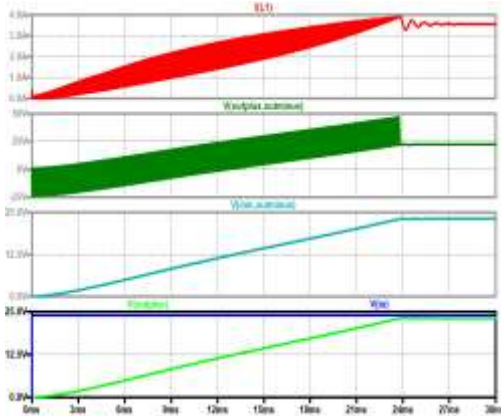
Fig. 22: Floating double Boost with additional inrush current reduction (with load), up to down: current through the first coil (red); output voltage (dark green); the voltage across the second capacitor(turquoise); input voltage (blue), the voltage across the first capacitor (green)

5 Floating Tristate Modified Double Boost Converter

5.1 Circuit

Another way to avoid the large inrush current is to modify the Boost stages. Instead of connecting the capacitors across the output of the Boost stages, one has to connect them between input and output as shown in Figure 23.
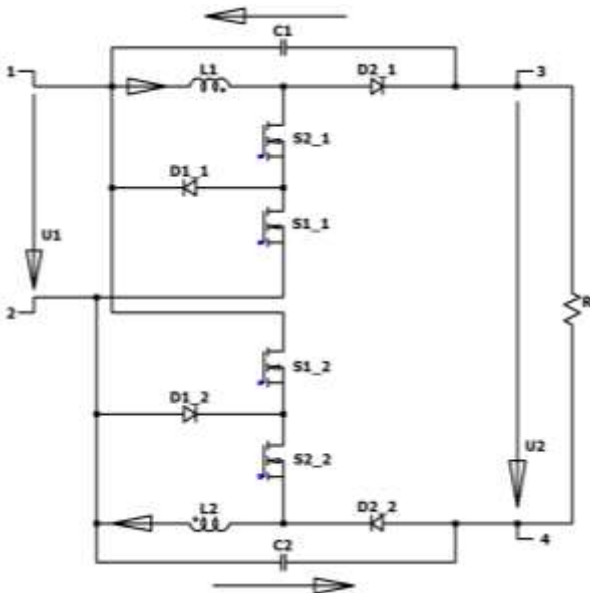
Fig. 23: Floating tristate modified double Boost converter

5.2 Inrush

Figure 24 shows the currents through the coils, the input, and the load. There is only a small ringing

and no dangerous current. The function is the same as was shown for the basic structure, but the input current is changed and the voltage stress across the capacitors is reduced to the difference between output and input voltages of the respective Boost parts. No negative output voltage occurs.
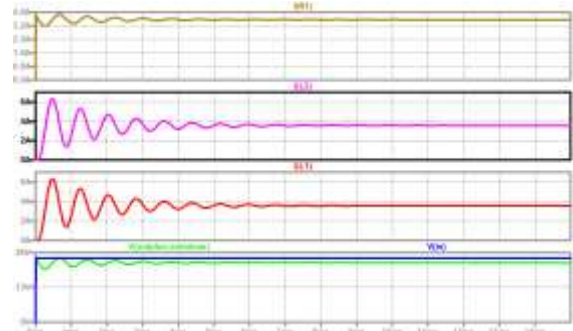
Fig. 24: Modified tristate floating double Boost converter with load, up to down: load current (brown); current through L2 (violet), current through L1 (red); input voltage (blue), output voltage (green).

5.3 Model of the Modified Converter

When the position of the capacitors is changed, the converter is modified. The model of the converter can be obtained in the same way as for the normal floating tristate Boost converter according to Figure 2 and results in:

$$\frac{d}{dt}\begin{pmatrix} i_L \\ u_C \end{pmatrix} = \begin{bmatrix} 0 & \dfrac{d_2-1}{L} \\ \dfrac{1-d_2}{C} & -\dfrac{2}{RC} \end{bmatrix} \begin{pmatrix} i_L \\ u_C \end{pmatrix} + \begin{bmatrix} \dfrac{d_1}{L} \\ -\dfrac{1}{RC} \end{bmatrix} (u_1). \quad (36)$$

Linearizing leads to the small signal model:

$$\frac{d}{dt}\begin{pmatrix} \hat{i}_L \\ \hat{u}_C \end{pmatrix} = \begin{bmatrix} 0 & \dfrac{D_{20}-1}{L} \\ \dfrac{1-D_{20}}{C} & -\dfrac{2}{RC} \end{bmatrix} \begin{pmatrix} \hat{i}_L \\ \hat{u}_C \end{pmatrix} +$$

$$+ \begin{bmatrix} \dfrac{D_{10}}{L} & \dfrac{U_{10}}{L} & \dfrac{U_{C0}}{L} \\ \dfrac{1}{RC} & 0 & -\dfrac{I_{L0}}{C} \end{bmatrix} \begin{pmatrix} \hat{u}_1 \\ \hat{d}_1 \\ \hat{d}_2 \end{pmatrix}$$

$$(37)$$

which leads to the same transfer functions. Only B_{11} and B_{13} change their values.
The output equation:

$$u_2 = \begin{bmatrix} 0 & 2 \end{bmatrix} \begin{pmatrix} i_L \\ u_C \end{pmatrix} + [1](u_1) \qquad (38)$$

leads to the output voltage.

6 Simulations

To prove the model a comparison with the simulation of the circuit is done.

Figure 25(a) shows the simulation with the small signal model with the help of the transfer functions. The change of the voltage across the capacitor is shown around the working point. It starts with a step-up of 1 % for the duty cycle d1, after 20 ms the d1 goes down by -1 %. After another 20 ms, the duty cycle d2 jumps up by 1 % and jumps back after 20 ms. After another 20 ms, the input voltage makes a step of plus 1 V and steps back after 20 ms. Figure 25(b) shows the results done by a simulation of the converter circuit. One can see that the dynamic behavior is very precisely modeled with the transfer functions. The converter is switched to 100 kHz and one can see the ripple of the current (one can see the band within which the current is changing).

(a)

(b)
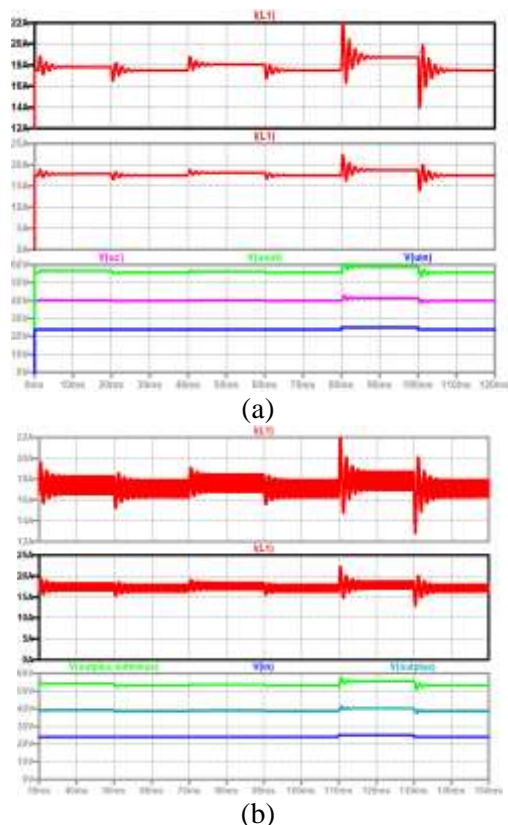
Fig. 25: Change of the capacitor voltage caused by steps every 20 ms, d1 up and down by 0.01, d2 up and down by 0.01, and U1 up and down by 1 V (up to down): changes of the current through L1 (red), current through L1 (red); output current (green), voltage across C1 (turquoise), input voltage (blue), a. small signal model, b—circuit simulation

The circuit simulation takes much longer (24 minutes, including 10 ms for the inrush, and 20 ms for start-up which are not shown in Figure 25) than

the simulation with transfer functions (a few seconds) on the used computer. Therefore, for the controller design the linear model would be used to check the results. The complete circuit simulation with inrush and soft-start is shown in Figure 26.
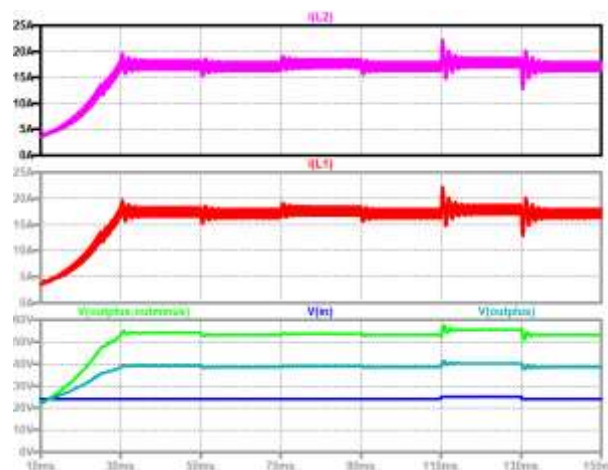
Fig. 26: Soft-start, steps of the duty cycle of d1 and d2 and steps of the input voltage (up to down): current through L2 (violet), current through L1 (red); output current (green), voltage across C1 (turquoise), input voltage (blue)

7 Conclusion

The combination of the tristate and the floating double converter concepts leads to a new and interesting DC/DC converter, especially useful for fuel-cell and DC-micro-grid supply, with useful features:

- High step-up ratio
- Linearization of the voltage transformation ratio, when the duty cycle of switch S2 is kept constant and the duty cycle of S1 is the variable
- The converter is a phase-minimum system in this case
- Reduction of the voltage transformation ratio and smoothing of the characteristics, when the duty cycle of S1 is kept constant and the control occurs with the duty cycle of S2, in this case, the converter is a non-phase minimum system
- Doubling the AC component of the input current, when the two converter stages are controlled with 180° shifted signals
- Changing the position of the capacitors according to Figure 23 avoids the inrush, when the converter is connected to a stiff input source, like batteries or a stable DC micro-grid, avoids also a negative output

voltage during turn-on, and reduces the voltage stress of the capacitors

- Symmetrical design and using the same duty cycles for the electronic switches in the two Boost stages reduces the converter to a second-order system
- The second mode of the converter can be additionally used to control the converter in the case of errors

The converter can be used also for charging batteries and to supply light-emitting diodes. In this case, an inductor should be connected in series to the load and the current through it has to be controlled. The floating output voltage can be used as the input of an isolated converter, e.g. a two-switch forward or flyback converter. It should be mentioned that the concept can be extended into a bidirectional system when the electronic switches and the diodes are replaced by current-bidirectional switches consisting of an electronic switch and an antiparallel diode. Furthermore, other tristate converter types as shown in [17], can be combined with the floating double converter concept.

References:
[1]   M. Miranda, P. Banakar, G. Gunnal and V. Kiran Kumar, Robust Voltage Control of Improved Floating Interleaved Boost Converter for Photovoltaic Systems, *2020 5th International Conference on Computing, Communication and Security (ICCCS)*, Patna, India, 2020, pp. 1-5, doi: 10.1109/ICCCS49678.2020.9276866.

[2]   M. Kabalo, D. Paire, B. Blunier, D. Bouquain, M. G. Simoes and A. Miraoui, Experimental Validation of High-Voltage-Ratio Low-Input-Current-Ripple Converters for Hybrid Fuel Cell Supercapacitor Systems, *IEEE Transactions on Vehicular Technology*, vol. 61, no. 8, pp. 3430-3440, Oct. 2012, doi: 10.1109/TVT.2012.2208132.

[3]   Liangcai Xu; Yigeng Huangfu; Rui Ma; Shengrong Zhuo; Dongdong Zhao; Jun Zhao; Fei Gao, Extended State Observer-Based Sliding-Mode Control for Floating Interleaved Boost Converters, *IECON 2018 - 44th Annual Conference of the IEEE Industrial Electronics Society*, Washington, DC, USA, 2018, pp. 5283-5289, doi: 10.1109/IECON.2018.8591138.

[4]   Qian Li; Yigeng Huangfu; Liangcai Xu; Jiang Wei; Rui Ma; Dongdong Zhao; Fei Gao, An Improved Floating Interleaved Boost Converter With the Zero-Ripple Input Current for Fuel Cell Applications, *IEEE Transactions on Energy Conversion*, vol. 34, no. 4, pp. 2168-2179, Dec. 2019, doi: 10.1109/TEC.2019.2936416.

[5]   P. Lin, W. Jiang, J. Wang, D. Shi, C. Zhang and P. Wang, Toward Large-Signal Stabilization of Floating Dual Boost Converter-Powered DC Microgrids Feeding Constant Power Loads, *IEEE Journal of Emerging and Selected Topics in Power Electronics*, vol. 9, no. 1, pp. 580-589, Feb. 2021, doi: 10.1109/JESTPE.2019.2956097.

[6]   M. G. Simões, C. L. Lute, A. N. Alsaleem, D. I. Brandao and J. A. Pomilio, Bidirectional floating interleaved buck-boost DC-DC converter applied to residential PV power systems, *2015 Clemson University Power Systems Conference (PSC)*, Clemson, SC, USA, 2015, pp. 1-8, doi: 10.1109/PSC.2015.7101675.

[7]   D. Coutellier, V. G. Agelidis and S. Choi, Experimental verification of floating-output interleaved-input DC-DC high-gain transformer-less converter topologies, *2008 IEEE Power Electronics Specialists Conference*, Rhodes, Greece, 2008, pp. 562-568, doi: 10.1109/PESC.2008.4591989.

[8]   M. Kabalo, B. Blunier, D. Bouquain and A. Miraoui, Comparaison analysis of high voltage ratio low input current ripple floating interleaving boost converters for fuel cell applications, *2011 IEEE Vehicle Power and Propulsion Conference*, Chicago, IL, USA, 2011, pp. 1-6, doi: 10.1109/VPPC.2011.6043101.

[9]   H. Sartipizadeh, F. Harirchi, M. Babakmehr and P. Dehghanian, Robust Model Predictive Control of DC-DC Floating Interleaved Boost Converter With Multiple Uncertainties, in *IEEE Transactions on Energy Conversion*, vol. 36, no. 2, pp. 1403-1412, June 2021, doi: 10.1109/TEC.2021.3058524.

[10]   P. Lin, W. Jiang, J. Wang, D. Shi, C. Zhang and P. Wang, Toward Large-Signal Stabilization of Floating Dual Boost Converter-Powered DC Microgrids Feeding Constant Power Loads, *IEEE Journal of Emerging and Selected Topics in Power Electronics*, vol. 9, no. 1, pp. 580-589, Feb. 2021, doi: 10.1109/JESTPE.2019.2956097.

[11]   K. Viswanathan, R. Oruganti and D. Srinivasan, Tri-state boost converter with no right half plane zero, *4th IEEE International Conference on Power Electronics and Drive*

Systems. IEEE PEDS 2001 - Indonesia. Proceedings (Cat. No.01TH8594), Denpasar, Indonesia, 2001, pp. 687-693 vol.2, doi: 10.1109/PEDS.2001.975402.

[12] K. Viswanathan, R. Oruganti and D. Srinivasan, A novel tri-state boost converter with fast dynamics, *IEEE Transactions on Power Electronics*, vol. 17, no. 5, pp. 677-683, Sept. 2002, doi: 10.1109/TPEL.2002.802197.

[13] S. K. Viswanathan, R. Oruganti and D. Srinivasan, Dual mode control of tri-state boost converter for improved performance, *IEEE 34th Annual Conference on Power Electronics Specialist, 2003. PESC '03*, Acapulco, Mexico, 2003, pp. 944-950 vol.2, doi: 10.1109/PESC.2003.1218182.

[14] A. Choubey and L. A. C. Lopes, A tri-state 4-switch bi-directional converter for interfacing supercapacitors to DC micro-grids, *2017 IEEE 8th International Symposium on Power Electronics for Distributed Generation Systems (PEDG)*, Florianopolis, Brazil, 2017, pp. 1-6, doi: 10.1109/PEDG.2017.7972507.

[15] Q. Wang and L. A. C. Lopes, Multi-Mode PWM Modulator for a 4-Switch DC-DC Converter Operating with Tri-State, *2023 IEEE 17th International Conference on Compatibility, Power Electronics and Power Engineering (CPE-POWERENG)*, Tallinn, Estonia, 2023, pp. 1-6, doi: 10.1109/CPE-POWERENG58103.2023.10227409.

[16] O. Knecht, D. Bortis and J. W. Kolar, ZVS Modulation Scheme for Reduced Complexity Clamp-Switch TCM DC–DC Boost Converter, *IEEE Transactions on Power Electronics*, vol. 33, no. 5, pp. 4204-4214, May 2018, doi: 10.1109/TPEL.2017.2720729.

[17] F. A. Himmelstoss, Tristate Converters, *WSEAS Transactions on Power Systems*, Vol. 18, 2023, pp. 259-269, https://doi.org/10.37394/232016.2023.18.27.

Contribution of Individual Authors to the Creation of a Scientific Article (Ghostwriting Policy)
The author contributed to the present research, in all stages from the formulation of the problem to the final findings and solution.

Conflict of Interest
The author has no conflicts of interest to declare.